PSFC/JA-03-4

Ion Cyclotron Range of Frequencies Mode Conversion Electron Heating in Deuterium-Hydrogen Plasmas in the Alcator C-Mod Tokamak

Y. Lin, S.J. Wukitch, P.T. Bonoli, E. Marmar, D. Mossessian, E. Nelson-Melbby[1], P. Phillips[2], M. Porkolab, G. Schilling[3], S. Wolfe, J. Wright

February 2003

Plasma Science and Fusion Center
Massachusetts Institute of Technology
Cambridge, MA 02139 USA

[1]Centre de Recherches en Physique des Plasmas, Association EURATOM – Confederation Suisse, Ecole Polytechnique Federale de Lausanne, CH-1015 Lausanne, Switzerland
[2]Fusion Research Center, University of Texas, Austin, TX 78712
[3]Princeton Plasma Physics Laboratory, Princeton, NJ 08543

This work was supported by the U.S. Department of Energy, Cooperative Grant No. DE-FC02-99ER54512. Reproduction, translation, publication, use and disposal, in whole or in part, by or for the United States government is permitted.

Submitted for publication to *Plasma Physics and Controlled Fusion.*

Ion Cyclotron Range of Frequencies Mode Conversion Electron Heating in Deuterium-Hydrogen Plasmas in the Alcator C-Mod Tokamak

Y. Lin[1], S. J. Wukitch[1], P. T. Bonoli[1], E. Marmar[1], D. Mossessian[1], E. Nelson-Melby[2], P. Phillips[3], M. Porkolab[1], G. Schilling [4], S. Wolfe[1], J. Wright[1]

[1] Plasma Science and Fusion Center, Massachusetts Institute of Technology, Cambridge, Massachusetts 02139, USA

[2] Centre de Recherches en Physique des Plasmas, Association EURATOM - Confédération Suisse, École Polytechnique Fédérale de Lausanne, CH-1015 Lausanne, Switzerland

[3] Fusion Research Center, The University of Texas, Austin, Texas 78712, USA

[4] Plasma Physics Laboratory, Princeton, New Jersey 08543, USA

Abstract

Localized direct electron heating by mode-converted ion cyclotron range of frequencies (ICRF) waves in D(H) tokamak plasmas has been clearly observed for the first time in Alcator C-Mod. Both on- and off-axis (high field side) mode conversion electron heating (MCEH) have been observed. The MCEH profile was obtained from a break in slope analysis of electron temperature signals in the presence of rf (radio frequency) shut-off. The temperature was measured by a 32-channel high spatial resolution ($\leq$ 7 mm) 2nd harmonic heterodyne electron cyclotron emission (ECE) system. The experimental profiles were compared with the predictions from a toroidal full-wave ICRF code TORIC. Using the hydrogen concentration measured by a high-resolution optical spectrometer, TORIC predictions were shown qualitatively in agreement with the experimental results for both on- and off-axis MC cases. From the simulations, the electron heating from mode converted ion cyclotron wave (ICW) and ion Bernstein wave (IBW) is examined.

1. Introduction

In ion cyclotron range of frequencies (ICRF) experiments, the fast magnetosonic wave (fast wave) launched by an rf (radio frequency) antenna in a multiple-species tokamak plasma can be mode converted (MC) to the ion Bernstein wave (IBW) and ion cyclotron wave (ICW) [1]. The MC process has been a useful tool in plasma control partly owing to its localized feature. It has been shown to generate plasma current, modify current profile, and potentially drive sheared plasma flow [2, 3, 4, 5]. All these applications are beneficial to advanced tokamak operation.

Although the mode converted ICW has been studied in other plasma confinement devices (for example, Ref. [6] on a mirror machine), it has only been recently experimentally detected in tokamak plasmas using a phase contrast imaging (PCI) system in Alcator C-Mod [7, 8]. The PCI observation indicated that the MC physics in a tokamak is more complicated than previously thought, in which only the fast wave and MC IBW were considered. The MC waves, IBW and ICW, are both strongly damped through electron Landau damping. As a result, the power carried by the MC waves results in direct electron heating in contrast to the minority ion cyclotron resonance heating. Modeling done along with the studies in references [7] and [8] indicated that the MC ICW may have comparable contribution to electron heating as the MC IBW in some circumstances. In this paper, we address two important issues in understanding the MC process: a detailed experimental measurement of mode conversion electron heating (MCEH) in D(H) plasmas, and a study of the power partition between the MC IBW and ICW.

The fast wave dispersion relation in a cold plasma regime can be written as

$$n_{\perp}^2 = \frac{(n_{\parallel}^2 - R)(n_{\parallel}^2 - L)}{S - n_{\parallel}^2},$$

where *R*, *L* and *S* are the dielectric tensor elements in the Stix notation [9], $n_{\perp} = k_{\perp} c/\omega$ is the refractive index perpendicular to the magnetic field, and $n_{\parallel} = k_{\parallel} c/\omega$ is the parallel refractive index. The cutoffs of the fast waves are located where $n_{\parallel}^2 = R$ and $n_{\parallel}^2 = L$. Considering the plasma finite temperature, the fast wave can be mode converted to hot

plasma waves near the ion-ion hybrid layer defined as $n_{\|}^2 = S$. On the high field side of this ion-ion hybrid layer, the fast wave can be converted to an IBW. On the low field side of this layer, the fast wave can be converted to an electromagnetic ICW of the species with higher charge-mass ratio. The ICW propagates approximately along a magnetic flux surface towards the low field side. In Fig. 1, we plot the approximate dispersion curves of the fast wave, ICW and IBW for a typical Alcator C-Mod D(H) discharge with moderate hydrogen concentration. The dispersion curves are obtained by solving a hot plasma full electromagnetic dispersion equation in cylindrical coordinates. Wave vector transformation due to the poloidal field is also considered. In this plasma, the ion-ion hybrid layer ($n_{\|}^2 = S$) is off-axis on the high field side of the magnetic axis ($R = R_0$), and the hydrogen ion cyclotron resonance layer, $\omega = \omega_{cH}$, is on-axis. The fast wave and IBW branches are calculated using plasma parameters on the mid-plane, while the ICW branch is obtained along the magnetic flux surface tangential to the ion-ion hybrid layer.

In previous experiments in Alcator C-Mod ($R \sim 0.67$ m, $a \sim 0.22$ m, $B_t \leq 8.1$ T) [10], the MCEH in D(^{3}He) and H(^{3}He) plasmas have been studied [11, 12, 13, 14]. Similar studies on ^{3}He(H) plasmas have also been done in the ASDEX Upgrade tokamak [15] and Tore Supra [16], and ^{4}He(^{3}He) in the Joint European Torus (JET) [17]. A study on D(H) plasmas in Alcator C-Mod has been reported [18]. The experimental MCEH profiles were compared with the predictions from a two-dimensional (2-D) toroidal full-wave ICRF code TORIC [19, 20]. Unlike the TORIC simulations, the measured power deposition profile lacked the evidence of localized electron absorption, possibly limited by the accuracy of the species concentration measurement and the spatial/temporal resolution of the temperature measurement.

In this paper, we present a study on D(H) plasmas with moderate hydrogen concentration (~20%). The problem of total mode conversion efficiency is very complicated, as is the power partition between the MC ICW and MC IBW. They generally depend on many parameters, such as species mixture, ion-ion hybrid layer location, cutoff layers location, and plasma current. Some preliminary studies based on TORIC modeling showed that the

mode conversion in typical D(H) or H(^{3}He) plasmas in Alcator C-Mod often results in significantly stronger electron heating from ICW than that in D(^{3}He). Choosing D(H) plasmas also allowed us to take advantage of a reliable n_H/n_D ratio diagnostic [21]. Therefore, we expected a typical D(H) plasma with a moderate hydrogen concentration in Alcator C-Mod would be a good candidate for the experimental MCEH study. The MCEH profile was calculated from a break in slope analysis of electron temperature signals in the presence of rf shut-off. The electron temperature was measured by a 32-channel high spatial resolution (≤ 7 mm) 2nd harmonic heterodyne electron cyclotron emission (ECE) system [22]. Compared with some early studies with D(H) plasmas [18, 23, 24] , this is the first time that a detailed MCEH study in tokamak D(H) plasmas is reported.

This paper is organized as follows. In section 2, the experimental method in obtaining the MCEH profile and TORIC modeling are described. In section 3, we compare the experimental results and TORIC predications for both on-axis and off-axis MC cases. The transport effect on the break in slope technique, and distinguishing the ICW and IBW contributions are discussed in section 4, followed by conclusions in section 5.

2. Method

2.1. Experiment

Alcator C-Mod has three fast wave antennas: Two 2-strap antennas (strap width 10 cm and separation of 25.75 cm) at D port and E port [25], and a 4-strap antenna (strap width 8 cm and separated at 18.6 cm center to center) at J port [26]. The D and E port antennas are operated at 80.5 MHz and 80 MHz respectively. The J-port antenna is operated at 70 MHz in the experiments reported here.

In the experiment for this D(H) mode conversion study, we ran plasma discharges in the low confinement mode (L-mode) at different hydrogen concentration levels. We also varied the magnetic field to change the location of the MC layer. In Fig. 2, the central density and temperature, hydrogen concentration n_H/n_e, and rf power of a typical

discharge studied are shown. The toroidal B field $B_0 \approx 5.27$ T at the magnetic axis ($R_0 \approx$ 0.68 m) during the flattop, and the plasma current I_p is 1.0 MA. The plasma has a central electron density of 1.7×10^{20} m^{-3}, and central electron temperature about 1.5 to 2.5 keV. The hydrogen concentration n_H/n_e in this discharge is in the range of 15% – 23%. This concentration is evaluated from the measured Balmer-α line ratio of D and H neutral particles at the plasma edge [21]. A constant hydrogen concentration is assumed for the entire plasma. In this discharge, J, D and E rf antennas are launched sequentially at a power level about 1.5 MW. When the J-port antenna is on, the ion-ion hybrid layer is near the magnetic axis $|r/a| < 0.05$. The layer is off-axis on the high field side at about r/a ~ 0.4 when the D-port or E-port antenna is on.

Because the rf power shut-off (≤ 10 microseconds) is nearly instantaneous compared to relevant plasma time-scales, we can use the break in slope technique to estimate the MCEH profile (rf power modulation was not available in this experiment). The rf power density ending in direct electron heating is approximately $\boldsymbol{S(r) \approx \frac{3}{2} n_e \Delta \frac{\partial T_e(r)}{\partial t}}$, where $\boldsymbol{\Delta \frac{\partial T_e}{\partial t}}$ is the difference of the slopes $\boldsymbol{\frac{\partial T_e}{\partial t}}$ before and after the rf power transition. In arriving at this equation, we have assumed that changes in other processes, such as radiated power, ohmic heating, and heating exchange between ions and electrons, are much slower than the time window used to calculate $\boldsymbol{\Delta \frac{\partial T_e}{\partial t}}$. The effect of energy transport on the break in slope technique is discussed in section 4. The fraction of rf power to electron heating is simply $\boldsymbol{\eta_e^{rf} = \int S(r) dV \Big/ P_{total}^{rf}}$, where the volume integration is performed based on the magnetic surfaces reconstructed by EFIT.

In Fig. 3, we show temperature signals from channel 27, 25, 23, 21, 19 and 15, corresponding to r/a = 0.02, 0.07, 0.12, 0.17, 0.23 and 0.28, of the 32-channel heterodyne ECE system around t_{rfoff} = 0.8744 sec, at which the J antenna power is shut off. The sampling rate of the ECE signal is 200 kHz. Two sawtooth crashes are shown in the figure at t_{rfoff} – 8.0 ms and t_{rfoff} + 1.4 ms. A clear break in slope is seen at t_{rfoff} in the

temperature signals near the magnetic axis (r/a < 0.2), while insignificant effect is seen in signals farther away from the axis. The slopes are estimated using a 3-parameter linear fit (2 lines connected at the rf transition time) on the data. We calculate the break in slope in three time windows [t_{start}, t_{end}], where $t_{start} = t_{rfoff} - 1.0$ ms, and $t_{end} = t_{rfoff} + 0.5$, 0.75, and 1.0 ms, and do a fitting-error weighted average. We also estimate the "noise floor" as the standard deviation of the spurious deposition profiles one would obtain by analyzing temperature signals that do not have an rf transition. To compensate the intrinsic sawtooth evolution, the same analysis is done on the previous two sawtooth oscillations at the corresponding time points, and the resulted break in slope is subsequently subtracted.

2.2. TORIC Modeling

The experimentally observed MCEH is also compared with the numerical modeling using a 2-D full-wave ICRF code TORIC [19, 20]. TORIC solves the 4th order finite Larmor radius wave equation that can resolve the fast wave, IBW, and ICW in 2-D tokamak geometry. Because of toroidal symmetry, the electric fields of different toroidal mode numbers are not coupled. For a toroidal mode number n_ϕ, the α-component of the electric field in TORIC is represented by a sum over poloidal Fourier modes:

$E_\alpha = \exp(in_\phi\phi)\sum_{m=-\infty}^{\infty} E_\alpha^m(n_\phi;\psi)\exp(im\theta)$, where θ and ϕ are poloidal and toroidal angles, m is the poloidal mode number, Ψ is a dimensionless variable labeling magnetic flux surfaces. The code has been recently improved to correctly calculate the IBW damping [11]. We use the toroidal spectra as shown in Fig. 4 to model the rf antennas in Alcator C-Mod. The spectra are calculated using the antenna strap geometry and also accounting for the thickness of the evanescent layer at the plasma edge. The dominant toroidal number for the J-port antenna is $n_\phi = 13$, and for D and E antennas, $n_\phi = 10$. To model the J-port antenna, we run TORIC separately using toroidal mode numbers of $\pm$ [4, 9, 10, 11, 12, 13, 14, 15,16 17], then sum over the TORIC results (equivalent antenna loading) weighted by the antenna toroidal spectra. For D and E antenna, we run toroidal mode

numbers of ± [2, 4, 6, 8, 10, 12, 14, 16]. The resulting power deposition profile is compared with the experimental MCEH profile.

3. Result

3.1. On-axis Mode Conversion

The MCEH profiles at t = 0.8744 sec of the plasma discharge of Fig. 2 is shown in Fig. 5, where the rf frequency is 70 MHz, and the hydrogen concentration is 19%. For this plasma, the ion-ion hybrid layer is very close to the magnetic axis for $n_\phi = 13$. The hydrogen ion cyclotron resonance layer is located at about r/a ~ 0.36 on the low field side. In order to avoid a convergence difficulty in TORIC simulation when the MC layer is exactly on-axis, we run the TORIC simulation with $B_0 = 5.2$ T instead of the experimental value of 5.27 T. The treatment shifts the TORIC result to the right by about r/a ~ 0.05. As shown in the figure, the TORIC simulation result is generally in agreement with the experimental result in the expected MC region near the magnetic axis. The integrated rf power fraction to electrons calculated from the experimental curve (0 < r/a < 0.25) is $\eta_e^{rf} \sim \mathbf{0.16}$, while the TORIC result is $\eta_e^{rf} \sim \mathbf{0.14}$.

The shaded area in Fig. 5 shows the "noise floor" of the break in slope method. The break in slope method is also subject to some other spurious effects, such as partial reconnection and heat pulse generated by the previous sawtooth crash. The apparent second peak on the experimental curve in the region of 0.25 < r/a < 0.45 may not be real. As shown in Fig. 3, a partial reconnection event at $t = t_{rfoff} - 2$ ms induces a large increase in the slope of the temperature signal of r/a = 0.28 prior to the rf transition. This slope increase, which does not appear in the previous sawtooth, may enhance the calculated break in slope at t_{rfoff}. Detailed study reveals that this partial reconnection event also affects other channels in the region of 0.25 < r/a < 0.45, while its effect is negligible on channels in r/a < 0.25 and r/a > 0.45. As a result, caution must be taken in interpreting the experimental result in this region.

In this on-axis mode conversion case, TORIC modeling suggests that the MCEH is primarily contributed by the IBW. Because a poloidal B field is necessary for the existence and propagation of the MCICW [1], the ICW branch is insignificant because of the small poloidal B field near the magnetic axis. In Fig. 6, two-dimensional contours of the power deposition density through electron Landau damping (ELD) S_{ELD} is plotted (n_ϕ = 13). The IBW deposits its power mostly on the high field side of the ion-ion hybrid layer ($R - R_0 \approx -1$ cm). The ICW deposits its power along the magnetic flux surface below the mid-plane for this positive n_ϕ. As shown in this figure, the IBW contribution to electron heating is about 2 orders of magnitude larger than that of the ICW.

3.2. Off-axis Mode Conversion

When the ion-ion hybrid layer is off-axis, it is generally more difficult to experimentally determine the MCEH profile due to a smaller MCEH power density. Fig. 7 shows the MCEH profiles at t = 1.5024 sec of the plasma discharge of Fig. 2. At this time, the rf frequency (E-port antenna) is 80 MHz, and the hydrogen concentration is 22.5%. The ion-ion hybrid layer is at r/a = 0.4 on the high field side of the magnetic axis for $n_\phi = 10$, and the hydrogen ion cyclotron resonance layer is near the axis. In the expected MC region near the ion-ion hybrid layer, the experimental measured profile agrees with the TORIC prediction in both width and height. The fraction of the rf power to electrons in the MC region, $0.35 \le r/a \le 0.7$, is $\eta_e^{rf} \sim \mathbf{0.20}$, while the TORIC prediction is $\eta_e^{rf} \sim \mathbf{0.18}$. The experimental result in this region is significantly higher the "noise floor" level (shaded area).

In Fig. 8, we plot the 2-D contour of S_{ELD} for the TORIC run at $n_\phi = 10$. The TORIC modeling clearly shows that the fast wave is converted into two waves, ICW and IBW. The dispersion curves of this scenario have already been shown in Fig. 1. The IBW is primarily on the high field side of the ion-ion hybrid layer ($R - R_0 \approx -9$ cm). The power deposition density of ICW, in contrast to that in Fig. 6, has a similar level as that of the IBW. The ELD of the fast wave is also shown, which is only significant near the hydrogen ion cyclotron resonance on the magnetic axis. In Fig. 9, we show the volume

integrated power deposition density vs. r/a after summing over TORIC runs at $n_\phi = \pm$ [2, 4, 6, 8, 10, 12, 14, 16]. The ICW and IBW deposition profiles peak at a similar r/a location. The fraction of rf power to the IBW is $\eta_{IBW}^{rf} \sim \mathbf{0.093}$, and to ICW $\eta_{ICW}^{rf} \sim \mathbf{0.087}$. There is a relatively small fraction of rf power in ELD through the fast wave near the magnetic axis. According to the simulation result, the fraction of rf power to ELD FW is about $\eta_{FW-ELD}^{rf} \sim \mathbf{0.03}$. Without experimentally measured ion information, it is difficult to determine the fraction of rf power that goes to minority heating. Based on the over-all power balance, most of the remaining rf power (~79%) must be deposited through multi-pass minority heating.

In order to show the MC process more clearly, we plot the contours of the E_z component from the TORIC simulation in Fig. 10. The unit of the field is kV/m per kA antenna current (the typical antenna current is several hundred amperes for 1 MW net rf power). The ICW is on the low field side of the ion-ion hybrid layer with a much larger E_z component than that of the IBW, mostly on the high field side of the ion-ion hybrid layer. The ICW has a higher level of E_z because it has a larger $n_{||}$ due to wave-vector transformation induced by the poloidal B field. It is worth pointing out that the E_z component is only a small fraction of the total electric field. For both ICW and IBW in this simulation, the maximum electric field strength $|E|_{max}$ is about 70 kV/m per kA antenna current. $|E|_{max}$ is about 2 orders of magnitude larger than their E_z components, which are less than 1 kV/m per kA antenna current. From the E_z contours, we can clearly see the MC ICW wave structure. It generally has a longer wavelength than the MC IBW, and propagates approximately along the magnetic flux surface tangential to the ion-ion hybrid layer. Were the ICW not totally damped through electron Landau damping along the path, it would be completely absorbed at the hydrogen cyclotron resonance layer near the magnetic axis.

4. Discussion

4.1. Transport effect on the break in slope technique

For the plasma studied, the energy transport may set a limit on the spatial resolution of the break in slope technique, thus preventing a more detailed comparison with TORIC modeling. For the plasma discharge shown in Fig. 2, we can use the time-to-peak analysis of a sawtooth crash to estimate the energy transport coefficient χ_e [27]. The analysis is in general valid in the region $r \geq r_{mix} \sim 1.4 r_{inv}$, where r_{mix} and r_{inv} are the mixing radius and inversion radius of the sawtooth respectively. For this plasma, r_{inv} is about 9 cm. In Fig. 11, we show the time-to-peak of the sawtooth crash at t = 1.49 sec, prior to the rf shut-off. A transport coefficient of 1.7 m^2/s is obtained using the approximation $\chi_e \approx r^2 / 9\Delta t_p$ as in Ref. [27].

To estimate the effect of the finite transport coefficient on the break in slope analysis, we model the transport process by solving a simplified transport equation in cylindrical coordinates

$$\frac{3}{2} n_e(r) \frac{\partial T_e(r,t)}{\partial t} = \frac{1}{r} \frac{\partial}{\partial r} \left[r n_e(r) \chi_e \frac{\partial T_e(r,t)}{\partial t} \right] + S_{non\_rf}(r) + S_{rf}(r),$$

where, n_e and T_e are the density and temperature profiles respectively, and $S_{non\_rf}(r)$ is estimated using the temperature profile at t = 0 and to minimize the profile evolution in the present of the rf term $S_{rf}(r)$. The form of $S_{non\_rf}(r)$ is shown to have insignificant effect on the result of break in slope. $S_{rf}(r)$ is the MCEH power density incorporated from the TORIC simulation. A constant χ_e in the entire plasma is assumed. We solve the transport equation from t = 0 to Δt with and without the $S_{rf}(r)$ term, then calculate the break in slope by comparing the two resulted temperatures $T_e(r, t)$. In Fig. 12, we show the power deposition profiles resulted from this simple model at different Δt. The input $S_{rf}(r)$ is also plotted. For a short time window, the figure shows that the break in slope technique is able to reproduce the power deposition profile with insignificant broadening. For large Δt, the energy transport can spread the localized MCEH to the point that the break in slope technique may incorrectly indicate a very broadened MC region. For example, in Fig. 12, it is shown that the technique may give a profile with a width more than twice the input $S_{rf}(r)$ if using $\Delta t \geq 2$ ms. Ideally, the shorter the time window, the closer the result can be compared to the 'real' MCEH profile. However, owing to the noise in the ECE

signals, the uncertainty of the linear-fit may become considerably large when the time window is too short. As a result, there has to be a trade-off between the uncertainty in the value and spatial resolution of the MCEH profile using the break in slope technique.

4.2. Distinguishing the MC IBW and MC ICW

Since the MCEH for the MC IBW and MC ICW are approximately on the same r/a, it is difficult to experimentally distinguish their contributions. We think that the task may also be difficult in other MC applications such as current drive and plasma poloidal flow drive. In this study, the contribution from the ICW is inferred from the agreement between the experimental result and the total MCEH from TORIC simulation. In Alcator C-Mod, the heterodyne PCI system can measure the vertical line-integrated density fluctuations induced by rf waves as demonstrated in Ref. [7, 8]. The PCI can, in principle, distinguish the two waves based on their differences in spatial location and wavelength. Unfortunately PCI was not available for this experiment. Future experiments will incorporate PCI measurements.

5. Conclusions

Localized MCEH in D(H) tokamak plasmas, both on- and off-axis mode conversion, has been observed clearly for the first time in Alcator C-Mod. The MCEH profile was obtained from a break in slope analysis of high spatial resolution electron temperature signals. The experimental MCEH profiles were in qualitative agreement with the predictions from TORIC modeling for both on- and off-axis MC cases. In the case of on-axis MC, TORIC simulation suggested that the MCEH heating was primarily contributed by the IBW. In the case of off-axis MC, TORIC modeling showed comparable contributions from the IBW and ICW to MCEH.

Acknowledgments

The authors thank the Alcator C-Mod operations for expert running the tokamak. This work is supported at MIT by U.S. Department of Energy Cooperative Agreement No. DE-FC02-99-ER54512.

References

1. F. W. Perkins, Nucl. Fusion **17**, 1197 (1977).
2. R. Majeski, J. H. Rogers, and S. H. Batha *et al*., Phys. Rev. Lett, **76 (5)**, 764 (1996).
3. J. R. Wilson, R. E. Bell, S. Bernabei *et al*., Phys. Plasma **5**, 1721 (1998).
4. L. A. Berry, E. F. Jaeger, and D. B. Batchelor, Phys. Rev. Lett, **82 (9)**, 1871 (1999).
5. C. K. Phillips, M. G. Bell, R. E. Bell, S. Bernabei *et al*., Nucl. Fusion **40**, No. 3Y, (463) 2000.
6. Y. Yasaka, H. Takeno, A. Fukuyama, T. Toyoda, M. Miyakita, and R. Itatani, Phys. Fluids B **4**, (1486) 1992.
7. E. Nelson-Melby, M. Porkolab, A. Mazurenko, Y. Lin, P. T. Bonoli, and S. J. Wukitch, *29th EPS Conference on Plasma Phys. and Contr. Fusion (Montreux)*, ECA Vol. **26B**, P-1.058 (2002).
8. E. Nelson-Melby, M. Porkolab, P. T. Bonoli, Y. Lin, A. Mazurenko, and S. J. Wukitch, submitted to Phys. Rev. Lett.
9. T. H. Stix, in *Waves in Plasmas* (American Institute of Physics, New York, 1992).
10. I. H. Hutchinson, R. L. Boivin, F. Bombarda *et al*., Phys. Plasmas **1**, 1511 (1994).
11. P. T. Bonoli, M. Brambilla, E. Nelson-Melby *et al*., Phys. Plasmas **7**, 1886 (2000).
12. P. T. Bonoli, P. O'Shea, M. Brambilla *et al*., Phys. Plasmas **4**, 1774 (1997).
13. P. J. O'Shea, PhD thesis, Massachusetts Institute of Technology (1997).
14. E. Nelson-Melby, PhD thesis, Massachusetts Institute of Technology (2001).
15. J-M. Noterdaeme, S. Wukitch, D. A. Hartmann *et al.*, *Proc. 16th IAEA Fusion Energy Conference (Montreal) IAEA-CN-64/F1-EP-4* (1996).
16. B. Saoutic, A. Becoulet, T. Hutter *et al*, Phys. Rev. Lett. **76** (10), 1647 (1996).
17. M. J. Mantsinen, M.-L. Mayoral, E. Righi *et al*, 14th Conference on Applications of Radio Frequency Power to Plasmas (American Institute of Physics Conference Proceedings 595, New York, 2001, p59).
18. G. Taylor, B. LeBlanc, C. K. Phillips *et al*, *13th Conference on Applications of Radio Frequency Power to Plasmas* (American Institute of Physics Conference Proceedings 485, New York, 1999, p490).
19. M. Brambilla, Nucl. Fusion **38**, 1805 (1998).
20. M. Brambilla, Plasma Phys. Control. Fusion, **41** (1), 1(1999).

21. T. E. Tutt, Department of Nuclear Engineering Master's thesis, Massachusetts Institute of Technology (1999). Also MIT PSFC/RR-99-11.
22. J. W. Heard, C. Watts, R. F. Gandy, P. E. Phillips *et al*, Rev. Sci. Instrum. **70** (1), 1011 (1999).
23. H. Akiyama, K. L. Wong, J. Gahl *et al*, Plasma Physics and Control. Fusion **29**, 93 (1987).
24. J. D. Jacquinot, B. D. Mcvey, and J. E. Sharer, Phys. Rev. Lett. **39**, 88 (1977).
25. Y. Takase *et al*., *Proc. 14th Symp. Fusion Engineering, San Diego (Piscataway, NJ):IEEE (1992),* p118.
26. S. J. Wukitch, R. L. Boivin, P. T. Bonoli *et al*, *Proc. 19th IAEA Fusion Energy Conference* (*Lyon) FT/P1-14 (2002).*
27. E. D. Fredrickson, J. D. Callen, K. McGuire *et al*, Nucl. Fusion 26 (7), 849 (1986).

Figure Captions:

Fig. 1. (Color) Approximate dispersion curves in the mode conversion region for the fast wave (FW), ion Bernstein wave (IBW) and ion cyclotron wave (ICW) in a D(H) plasma in Alcator C-Mod. Plasma parameters: $B_0 = 5.27$ T, $I_p = 1$ MA, $R_0 = 0.68$ m, $a = 0.22$ m, $n_{e0} = 1.8 \times 10^{20}$ m^{-3}, $T_e = 2$ keV, 22.5 % H, and 77.5% D. The rf frequency $f_{rf} = 80$ MHz, and toroidal mode number $n_\phi = 10$.

Fig. 2. (Color) Plasma parameters of a typical high H concentration D(H) plasma discharge in Alcator C-Mod. The hydrogen concentration is defined as n_H/n_e. The plasma is in L-mode with $B_0 = 5.27$ T and $I_p = 1$ MA.

Fig. 3. (Color) Six of the 32-channel electron temperature signals (channel 27, 25, 23, 21, 19 and 17) around the time of rf shut-off, $t_{rfoff} = 0.8744$ sec, for the discharge of Fig. 2. Break in slope is clearly seen in signals near the magnetic axis.

Fig. 4. Toroidal spectra of the rf antennas in Alcator C-Mod. J-port antenna is in [0,π, 0,π] configuration while D and E antennas are in [0, π] configuration.

Fig. 5. (Color) The MCEH profiles for the case of on-axis mode conversion. The experimental result is obtained around t = 0.8744 sec of the discharge of Fig. 2. The shaded area is the 'noise floor' level of the break in slope method. Plasma parameters: 19% H, 79% D, and $f_{rf} = 70$ MHz.

Fig. 6. (Color) S_{ELD} contour from TORIC simulation ($n_\phi = 13$) for the on-axis mode conversion. S_{ELD} has units of MW/m^3 per m^2 area per MW antenna input power, and is plotted on a logarithmic scale. The lowest contour level of the left figure is omitted.

Fig. 7. (Color) The MCEH profiles for the case of off-axis mode conversion. The experimental result is obtained around t = 1.5024 sec of the discharge of Fig. 2. Plasma parameters: 22.5% H, 77.5% D, and $f_{rf} = 80$ MHz.

Fig. 8. (Color) S_{ELD} contour from TORIC simulation ($n_\phi = 10$) for the off-axis mode conversion. S_{ELD} has units of MW/m^3 per m^2 area per MW antenna input power, and is plotted on a logarithmic scale. The lowest contour level of the left figure is omitted.

Fig. 9. (Color) The power partition between ICW, IBW, and FW direct electron heating (EH) as calculated from TORIC in the off-axis MC case. The total EH curve is the same as that in Fig. 7.

Fig. 10. (Color) E_z field contour from TORIC simulation ($n_\phi = 10$) for the off-axis mode conversion. The unit of the field is kV/m per kA antenna current.

Fig. 11. Time-to-peak vs. r^2 at a sawtooth crash at t = 1.490 sec of the plasma discharge of Fig. 2. The transport coefficient χ_e is calculated from the linear-fit $\chi_e \approx \Delta r^2 / 9\Delta t_p$.

Fig. 12. Transport effect on the break in slope technique. At $\Delta t \rightarrow 0$, the break in slope technique can reproduce the input TORIC profile. At large Δt, the result may be significantly broadened. A boundary at r/a = 0.01 is used in the modeling.

Figures

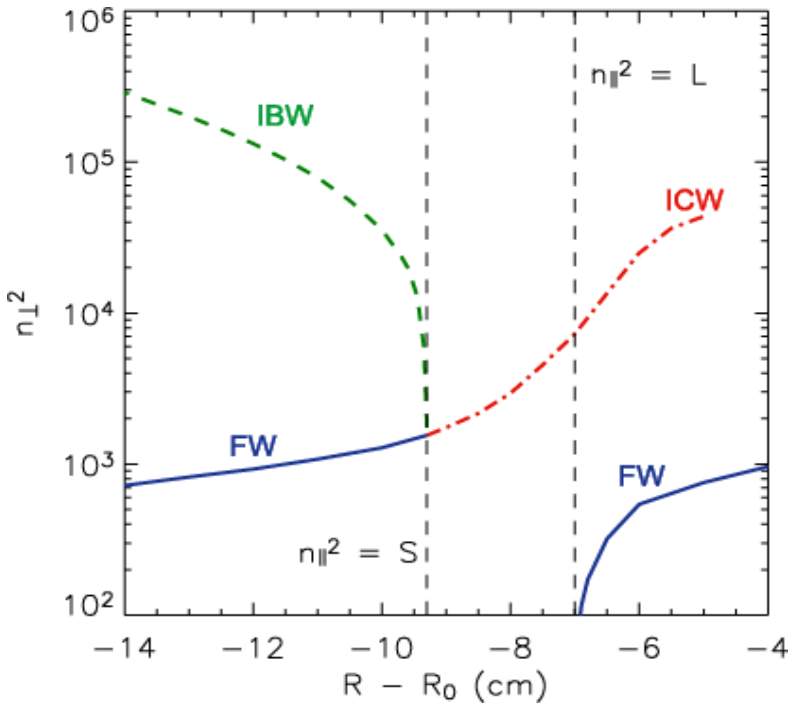

Fig. 1

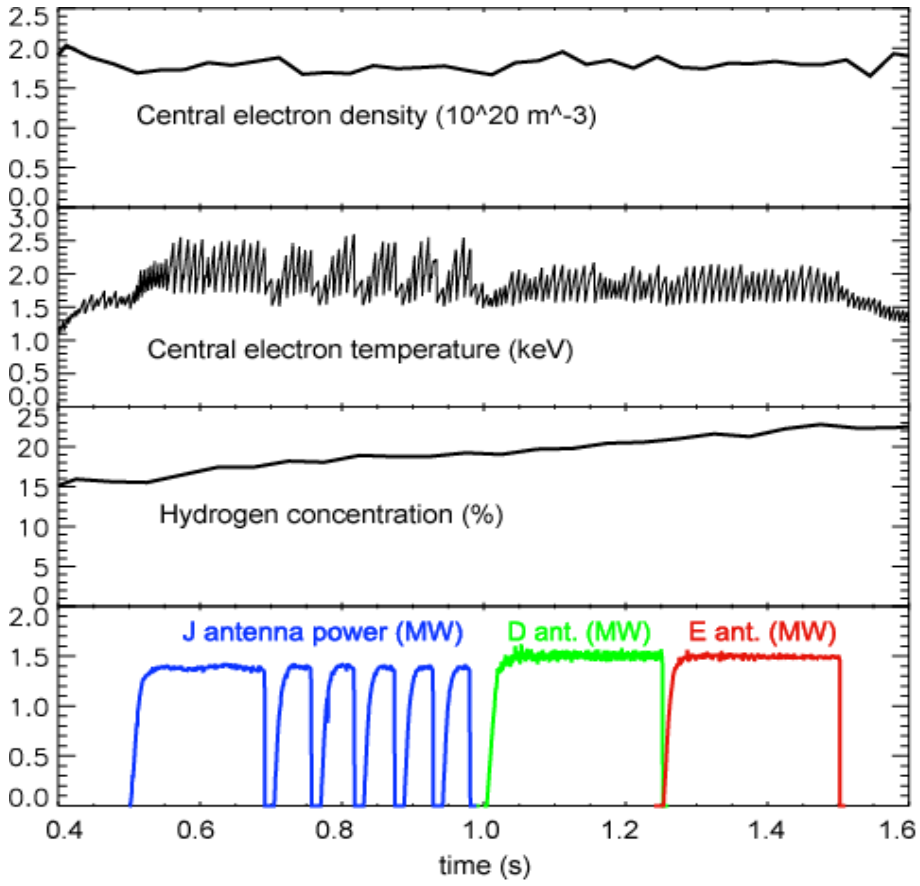
Central electron density (10^20 m^-3)
Central electron temperature (keV)
Hydrogen concentration (%)
J antenna power (MW)
D ant. (MW)
E ant. (MW)
time (s)

Fig. 2

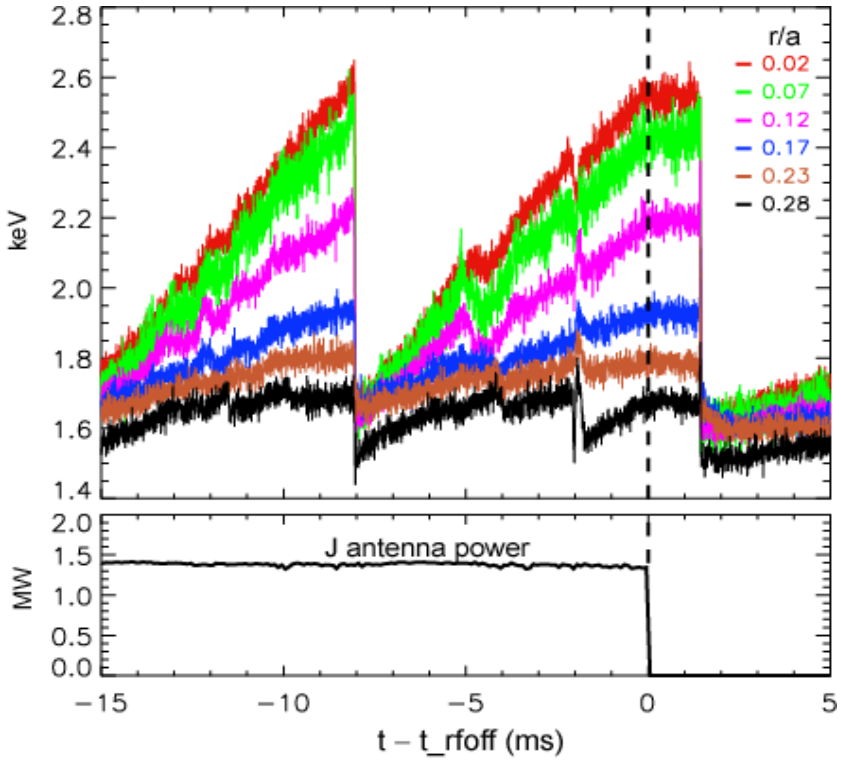
r/a
0.02
0.07
0.12
0.17
0.23
0.28
keV
2.8
2.6
2.4
2.2
2.0
1.8
1.6
1.4
J antenna power
MW
2.0
1.5
1.0
0.5
0.0
−15
−10
−5
0
5
t − t_rfoff (ms)

Fig. 3

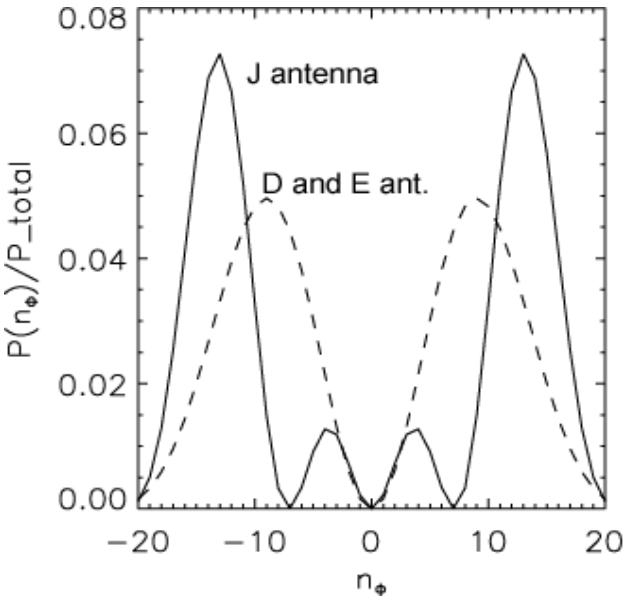
0.08
0.06
0.04
0.02
0.00
J antenna
D and E ant.
P(nΦ)/P_total
−20
−10
0
10
20
nΦ

Fig. 4

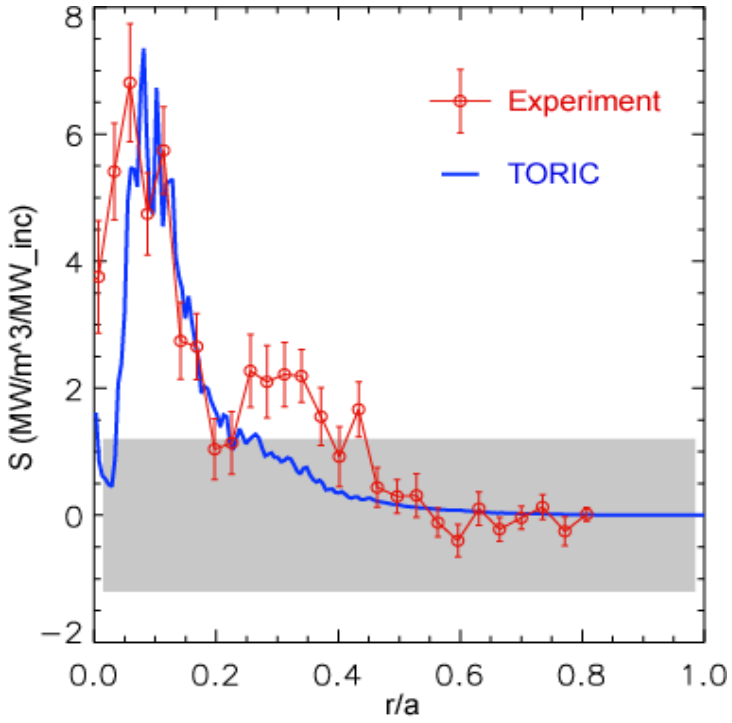

Fig. 5

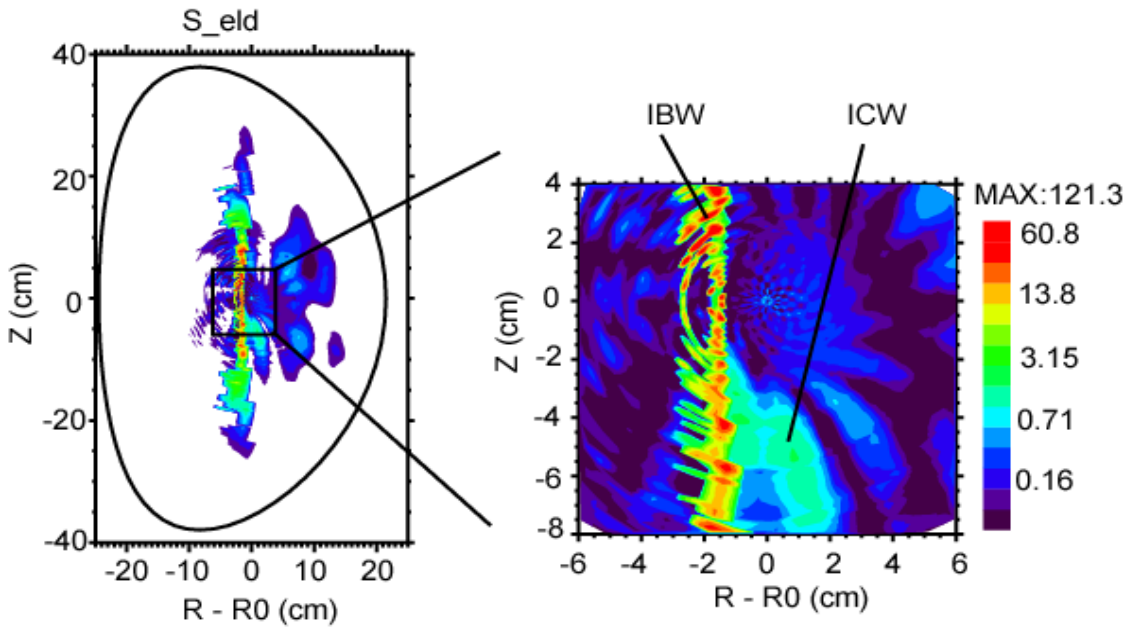
S_eld
40
20
0
-20
-40
Z (cm)
-20 -10 0 10 20
R - R0 (cm)
IBW
ICW
4
2
0
-2
-4
-6
-8
Z (cm)
-6 -4 -2 0 2 4 6
R - R0 (cm)
MAX:121.3
60.8
13.8
3.15
0.71
0.16

Fig. 6

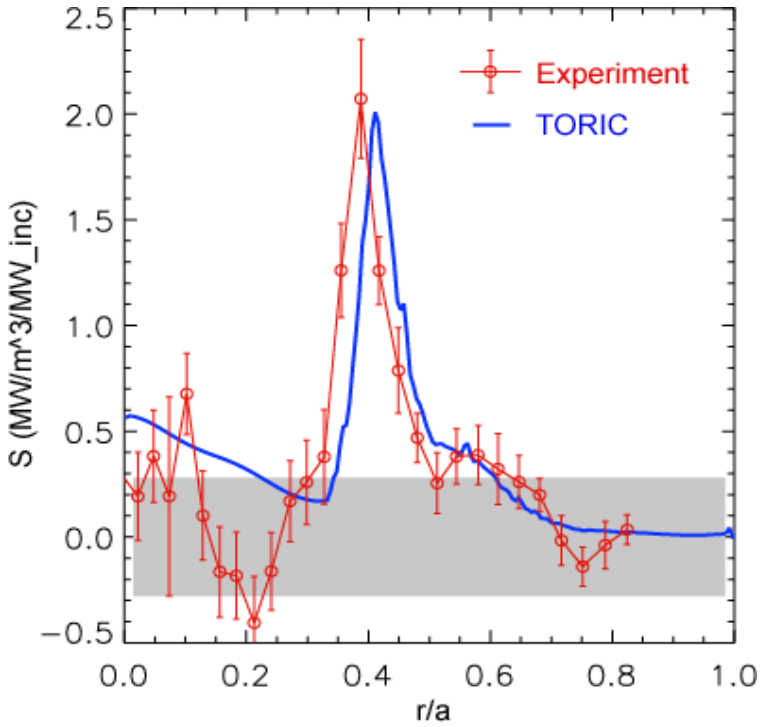
Experiment
TORIC
S (MW/m^3/MW_inc)
r/a
2.5
2.0
1.5
1.0
0.5
0.0
−0.5
0.0
0.2
0.4
0.6
0.8
1.0

Fig. 7

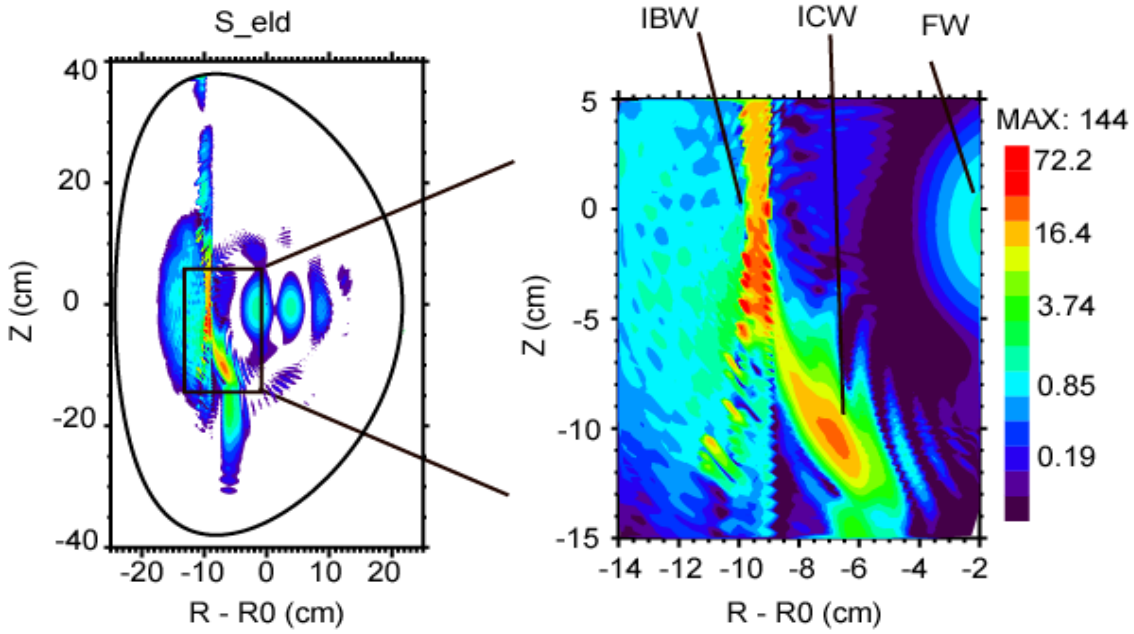
S_eld
40
20
0
-20
-40
Z (cm)
-20 -10 0 10 20
R - R0 (cm)
IBW
ICW
FW
5
0
-5
-10
-15
Z (cm)
-14 -12 -10 -8 -6 -4 -2
R - R0 (cm)
MAX: 144
72.2
16.4
3.74
0.85
0.19

Fig. 8

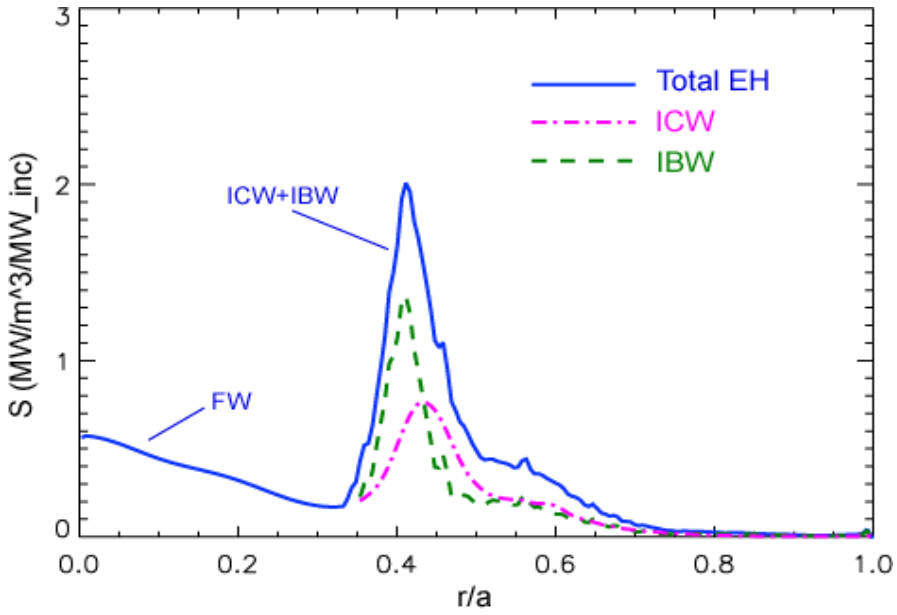

Fig. 9

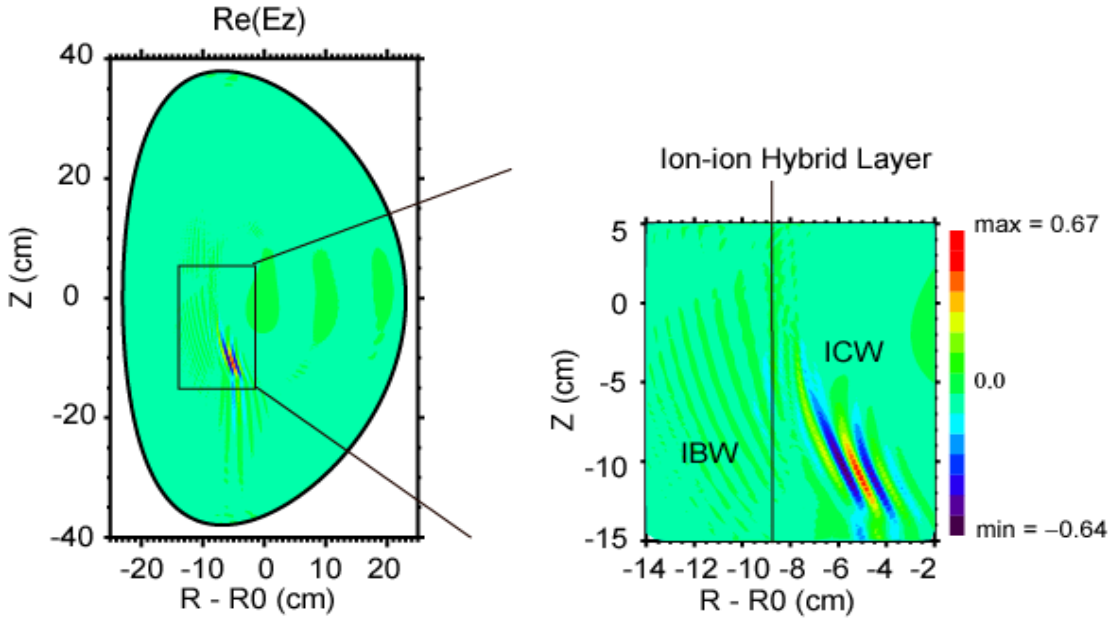

Fig. 10

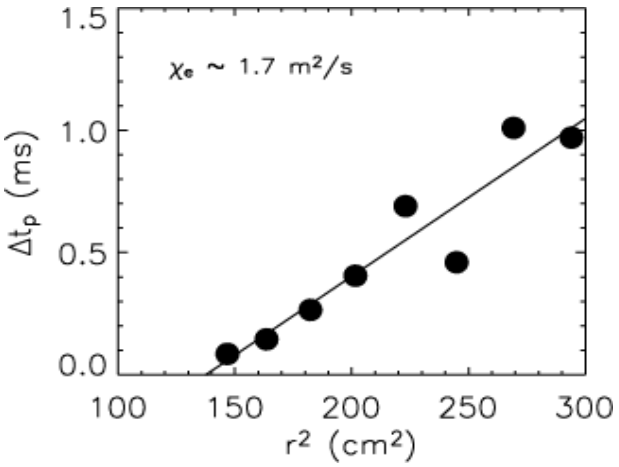
$\chi_e \sim 1.7$ m²/s
Δt_p (ms)
r² (cm²)
1.5
1.0
0.5
0.0
100
150
200
250
300

Fig. 11

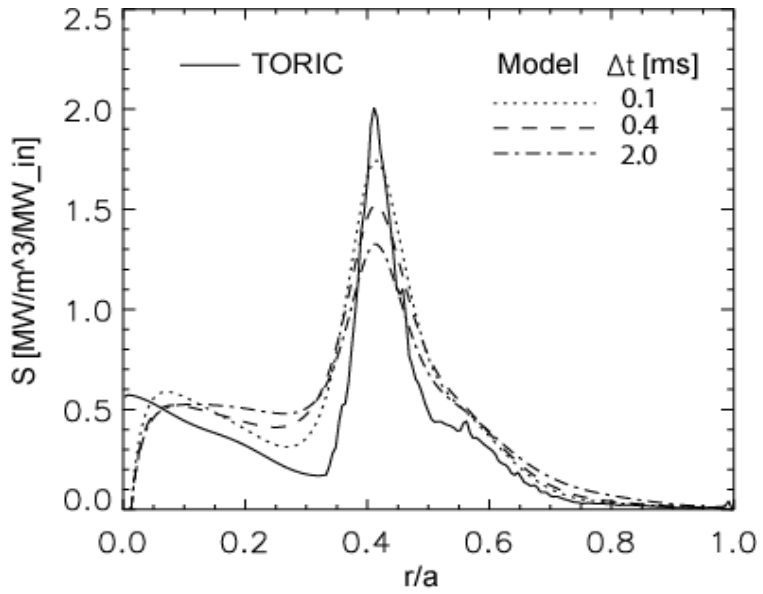
TORIC
Model Δt [ms]
0.1
0.4
2.0
S [MW/m^3/MW_in]
r/a
2.5
2.0
1.5
1.0
0.5
0.0
0.0
0.2
0.4
0.6
0.8
1.0

Fig. 12